Metal-Hydrogen-Pi-Bonded Organic Frameworks

Journal:	*Dalton Transactions*
Manuscript ID	DT-ART-12-2021-004278
Article Type:	Paper
Date Submitted by the Author:	20-Dec-2021
Complete List of Authors:	Zhu, Jie; UC San Diego, Chemistry and Biochemistry Samperisi, Laura; Uppsala Universitet Chiong, Jerika; Stanford University Kalaj, Mark; University of California, San Diego, Dept. of Chemistry and Biochemistry Bailey, Jake B; UCSD Zhang, Zhiyin; UC San Diego, Chemistry and Biochemistry Yu, Chung-Jui; UC San Diego, Chemistry and Biochemistry Sikma, Eric; UC San Diego, Chemistry and Biochemistry Zou, Xiaodong; Stockholm University, Department of Materials and Environmental Chemistry Cohen, Seth; University of California, San Diego, Dept. of Chemistry and Biochemistry Huang, Zhehao; Stockholm University, Department of Materials and Environmental Chemistry Tezcan, Faik; UC San Diego, Chemistry and Biochemistry

ARTICLE

Metal-Hydrogen-Pi-Bonded Organic Frameworks

Jie Zhu[a‡], Laura Samperisi[b‡], Mark Kalaj[a], Jerika A. Chiong[a], Jake B. Bailey[a], Zhiyin Zhang[a], Chung-Jui Yu[a], R. Eric Sikma[a], Xiaodong Zou[b], Seth M. Cohen[b], Zhehao Huang[b*], F. Akif Tezcan[b*]

Received 00th January 20xx,
Accepted 00th January 20xx

DOI: 10.1039/x0xx00000x

We report the synthesis and characterization of a new series of permanently porous, three-dimensional metal-organic frameworks (MOFs), M-HAF-2 (M = Fe, Ga, or In), constructed from tetratopic, hydroxamate-based, chelating linkers. The structure of M-HAF-2 was determined by three-dimensional electron diffraction (3D ED), revealing a unique interpenetrated **hcb**-a net topology. This unusual topology is enabled by the presence of free hydroxamic acid groups, which lead to the formation of a diverse network of cooperative interactions comprising metal-hydroxamate coordination interactions at single metal nodes, staggered π–π interactions between linkers, and H-bonding interactions between metal-coordinated and free hydroxamate groups. Such extensive, multimodal interconnectivity is reminiscent of the complex, noncovalent interaction networks of proteins and endows M-HAF-2 frameworks with high thermal and chemical stability and allows them to readily undergo postsynthetic metal ion exchange (PSE) between trivalent metal ions. We demonstrate that M-HAF-2 can serve as versatile porous materials for ionic separations, aided by one-dimensional channels lined by continuously π-stacked aromatic groups and H-bonding hydroxamate functionalities. As an addition to the small group of hydroxamic acid-based MOFs, M-HAF-2 represents a structural merger between MOFs and hydrogen-bonded organic frameworks (HOFs) and illustrates the utility of non-canonical metal-coordinating functionalities in the discovery of new bonding and topological patterns in reticular materials.

Introduction

Metal-organic frameworks (MOFs) are crystalline porous materials constructed from inorganic nodes and organic linkers.[1, 2] According to the Cambridge Crystallographic Data Centre (CCDC), more than 70,000 MOF structures[3] have been reported with applications proposed in gas storage and separation,[4-7] biomedical imaging and drug delivery,[8, 9] molecular sensing,[10, 11] and catalysis.[12-14] To date, most MOFs have relied on the combination of carboxylate- or azole-based linkers and polynuclear metal clusters as secondary building units (SBUs)[15], such as MOF-5,[16] and the MIL (Material Institute Lavoisier),[17, 18] UiO (University of Oslo),[19] NU (Northwestern University),[20] and PCN (porous coordination network)[21] series. Expanding upon the existing repertoire of MOF topologies may engender new emergent properties within these reticular materials.[22, 23] Exciting possibilities to create new materials with different functions including selective gas adsorption for chemical separations[24, 25] or introducing catalytic sites.[26]

Despite the central role of chelating groups in synthetic inorganic chemistry, linkers with multidentate functionalities are sparingly employed for MOF construction. This is likely due the fact that chelating linkers tend to yield SBUs with low connectivity, in addition to the possibility that their relatively slower metal exchange kinetics (compared to carboxylates or azoles) may hinder the formation of crystalline frameworks. Yet, given the remarkable structural and functional/electronic diversity of metal-chelate coordination complexes[27, 28], the use of chelating motifs in MOF construction represents a potentially powerful strategy for the discovery of MOFs with new structures/topologies and chemical/physical properties.[29-36]

Accordingly, we have begun to explore organic linkers bearing hydroxamate chelating motifs in MOF construction. Hydroxamates are hard, Lewis basic, bidentate ligands that form exceptionally stable coordination complexes with transition metal ions such as Fe^{3+}, Ga^{3+} and Al^{3+},[37] as demonstrated by bacterial siderophores.[38-40] Unlike carboxylate groups, hydroxamates allow asymmetric binding modes with metal ions and favor the formation of single metal nodes over polynuclear SBUs. To date, only four MOFs[41-44] containing hydroxamate ligands have been reported, with only two[41, 42] having 3D framework structures.

Previously, we reported the first Fe-hydroxamate-based MOF (Fe-HAF-1), using biphenyl tetrahydroxamic acid (H_4BPTH) as the linker and a single Fe^{3+} center as the node (Fig. 1).[42] The1, 3 positioning of the hydroxamic groups on the phenyl rings coupled with the octahedral Fe-tris-hydroxamate coordination gave rise to the formation of tetrahedral, four-iron-six-linker clusters (as first reported by Raymond and colleagues)[45] as supramolecular SBUs which were interconnected to yield the desired cubic, 3D framework structure. Despite featuring single-metal nodes, Fe-HAF-1 was found to display exceptional

---

[a] *Department of Chemistry and Biochemistry, University of California, San Diego, 9500 Gilman Drive, La Jolla, CA 92093*
[b] *Department of Materials and Environmental Chemistry, Stockholm University, Stockholm SE-106 91, Sweden*

Electronic Supplementary Information (ESI) available: [Materials and methods, synthesis and full characterization for ligands, M-HAF-2, 3D ED analysis data for Fe-HAF-2, SEM, TGA, zeta potential, gas adsorption, chemical stability, dye uptake properties and PSE of M-HAF-2 (PDF)]. See DOI: 10.1039/x0xx00000x

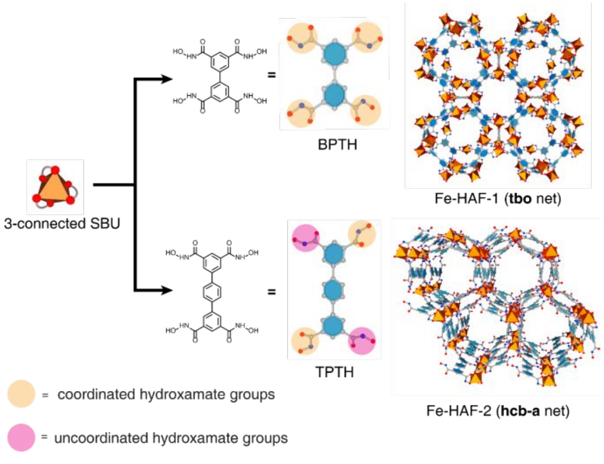

Fig. 1 Assembly of BPTH or TPTH with 3-connected SBUs lead to **tbo** net (Fe-HAF-1) or **hcb-a** net (Fe-HAF-2).

chemical stability maintaining crystallinity in aqueous solutions at pH 1-14, as well as in the presence of coordinating solvents.

In the current study, we set out to investigate whether we could extend the pore and aperture size of Fe-HAF-1 and expand the library of hydroxamate-based MOFs. Toward this end, we synthesized a longer linker (terphenyl tetrahydroxamic acid, H_4TPTH). However, instead of the expected isoreticular expansion of Fe-HAF-1, we obtained a new series of MOFs, denoted as M-HAF-2 (M = Fe, Ga, In), which possess an unusual interpenetrated **hcb**-a net topology, wherein the tetratopic linkers (H_4TPTH) are two-connected and act as ditopic linkers with two remaining uncoordinated hydroxamate groups (Fig. 1). Interestingly, the uncoordinated hydroxamic acid groups form intermolecular hydrogen bonds (H-bonds) with metal-coordinated hydroxamate groups within the framework that are further buttressed by extensive π–π interactions. Compared to Fe-HAF-1, which is only supported by coordination bonds, the synergy between three different types of interactions (metal coordination, π–π, and H-bonding) results in a porous framework material that is both chemically and physically stable, retains its crystallinity after activation, and can be prepared *de novo* using different hard metal ions or readily undergo postsynthetic metal exchange (PSE). It is worth noting that the combination of two different types of interactions is commonly seen in porous frameworks. For example, the combination of metal-coordination with π–π interactions is often observed in the interpenetrated MOFs[46], and the co-existence of H-bonding and π–π interactions is a key feature in most HOFs[47-51], and some MOFs[52, 53] with free functional groups involved in H-bonding in addition to metal coordination. However, to the best of our knowledge, the combination of three different types of interactions in M-HAF-2 in a cooperative way is unprecedented. With its unusually intricate network of non-covalent interactions, Fe-HAF-2 represents an amalgamation of MOFs and H-bonded organic frameworks (HOFs), utilizing all of the same interactions for structural stabilization found in proteins. In general, our study illustrates the benefits of expanding the toolkit of metal coordinating functionalities for the discovery of new structure/bonding modalities in MOF design.

Results and discussion

Synthesis and Structure of M-HAF-2.

All members of the M-HAF-2 library were synthesized by combining the H_4TPTH linker with the appropriate trivalent metal salt ($FeCl_3$, $GaCl_3$ or $InBr_3$) in a mixture of DEF and ACN at elevated temperature (60-100 °C). All three M-HAF-2 species were isolated as microcrystals (≤2 µm wide and ≤20 µm long) with a hexagonal rod-like morphology (Fig. S2) that was quite distinct from the cube-shaped Fe-HAF-1 crystals. These observations suggested that M-HAF-2 were likely not isoreticular with Fe-HAF-1. Indeed, 3D ED and powder X-ray diffraction (PXRD) analysis of Fe-HAF-2, Ga-HAF-2, and In-HAF-2 frameworks, which were determined to be isostructural, indicated a trigonal space group (Fig. S3, S4 and Fig. 2a). The porosities of M-HAF-2 frameworks were investigated by N_2

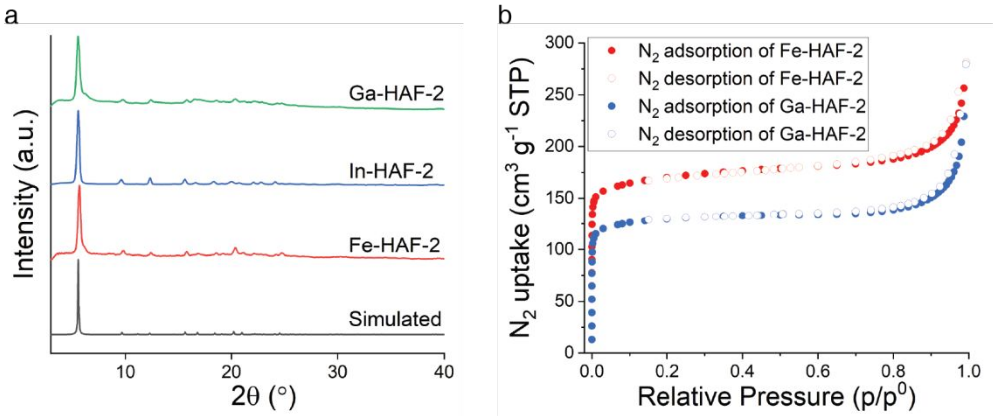

Fig. 2 a) PXRD patterns of Fe-HAF-2, Ga-HAF-2, and In-HAF-2. b) N2 sorption isotherms of Fe-HAF-2 and Ga-HAF-2 measured at 77 K.

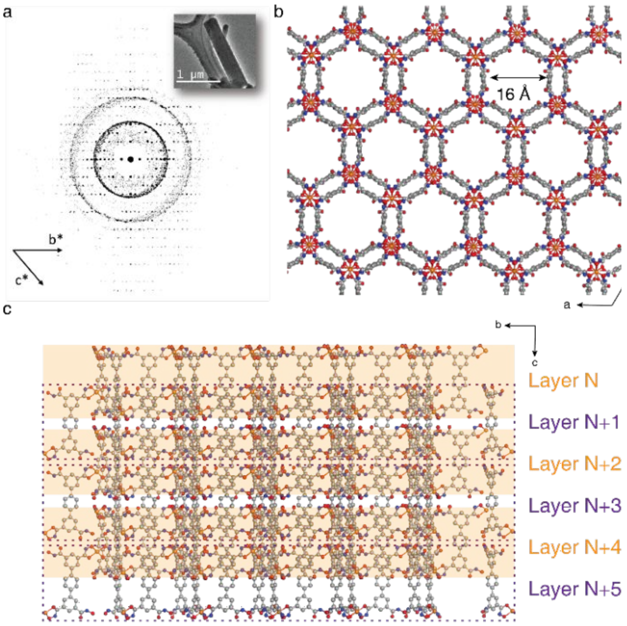

Fig. 3 a) The reconstructed 3D reciprocal lattice of Fe-HAF-2 viewing along the [100] plane. Scattering rings generated from ice can be observed in the background. The inset is the TEM image of the crystal showing a rod-like morphology. b) Structural model of Fe-HAF-2 viewed along the [001] direction. c) Structural model of Fe-HAF-2 viewed along [100] direction. Even layers (N, N+2, N+4) highlighted by orange boxes and odd layers (N+1, N+3, N+5) highlighted by purple dashed lines.

adsorption measurements at 77 K. As shown in Fig. 2b, the N_2 sorption of Fe-HAF-2 and Ga-HAF-2 exhibited a reversible type I behavior, and the calculated BET surface areas were 647 m^2/g and 501 m^2/g, respectively. Despite In-HAF-2 being isostructural with Fe-HAF-2 and Ga-HAF-2, In-HAF-2 exhibited negligible N_2 uptake at 77 K, suggestive of reduced stability during the activation steps (Fig. S5).

M-HAF-2 crystals were too small for single-crystal X-ray diffraction experiments. 3D electron diffraction (ED) methods, especially the continous rotation electron diffraction (cRED) protocol, has shown to be powerful for studying MOF microcrystals.[54, 55] We applied cRED to determine the atomic structure of Fe-HAF-2. The 3D reciprocal space reconstructed from the cRED data shows that Fe-HAF-2 crystallizes in a trigonal space group of $P\bar{3}c1$ (No.165), with the unit cell parameters of a =18.20 Å, and c = 16.17 Å (Fig. S3), which were further refined to a = 18.263(2) Å and c = 16.177(2) Å against PXRD data by using Pawley fitting (Table S1). The structure was solved *ab initio* by a dual-space method, with all non-hydrogen atoms located directly. The structure model was subsequently refined against cRED data (Fig. 3), which converged to an R_1 value of 0.209 for 612 reflections with $Fo > 4\sigma(Fo)$ and 0.3285 for all 1634 reflections (Table S2). Pawley fitting of the PXRD pattern with the unit cell determined by cRED captures all observed diffraction peaks (Fig. S4), confirming the phase-pure nature of the materials synthesized.

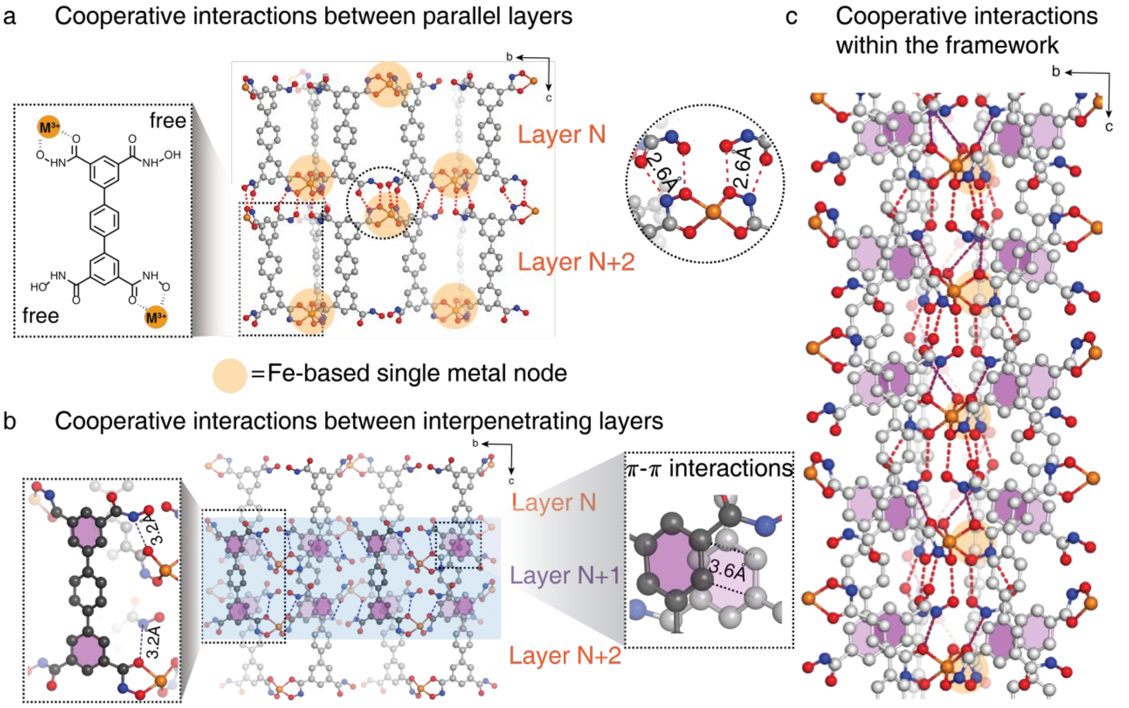

Fig. 4 Overview of the different bonding interactions within Fe-HAF-2. a) Cooperative interactions including intralayer metal-ligand coordination interactions (orange) in the N and N+2 layers and interlayer H-bonding (red dashed lines) between N and N+2 layers. b) π–π interactions (purple) and H-bonding (purple dashed lines) between layer N+1 and layers N and N+2. c) Cooperative interactions within the 3D framework. Within each SBUs, there are nine intermolecular hydrogen bonds (red and purple dashed lines) that extend to form a continuous 1D network along the *c* axis.

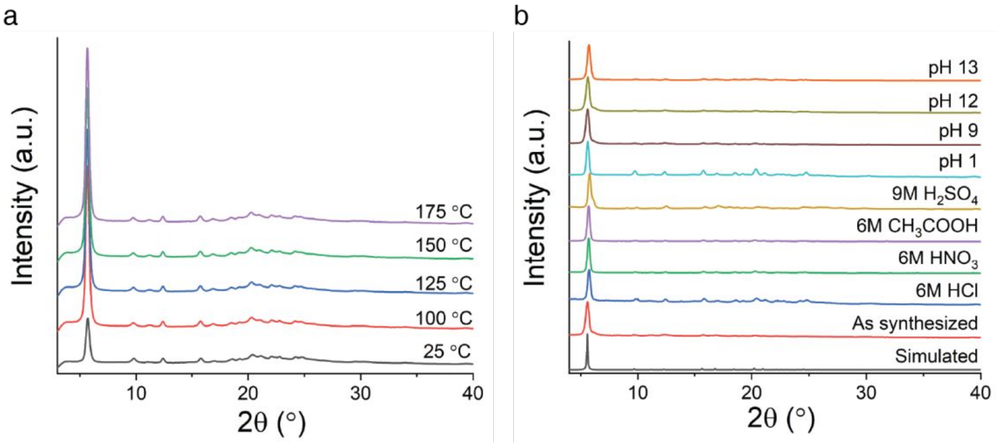

Fig. 5 a) In situ temperature-dependent PXRD patterns of Fe-HAF-2 from 25–175°C. b) PXRD patterns of Fe-HAF-2 after exposure to different aqueous solutions.

The structure of Fe-HAF-2 is built by Fe^{3+} cations and H_2TPTH^{2-} hydroxamate groups, whereby each Fe^{3+} cation is coordinated by three hydroxamate groups as a single node in an octahedral geometry. Interestingly, only two of the four hydroxamate/hydroxamic acid groups in each linker are observed to participate in Fe^{3+} coordination to form 2D hexagonal layers (Fig. 3b); these 2D layers are tightly interpenetrated along the c-axis as shown in Fig. 3c. As viewed down the *c* axis, the 3D framework is composed of double-walled hexagonal pores with an accessible pore diameter of 16 Å (Fig. 3b). The composition of Fe-HAF-2 framework is $Fe_2(H_2TPTH)_3$.

To describe the Fe-HAF-2 structure in more detail, it is useful to consider the framework as being composed of even- (N, N+2, N+4…) and odd-numbered (N+1, N+3, N+5...) hexagonal layers (Fig.s 3 and 4). Each even (or odd) layer has the height of a single H_4TPTH linker and is formed in the *bc* plane, wherein the linkers are interconnected by coordination between Fe^{3+} ions and two hydroxamate groups on each linker (Fig. 4a). Consecutive even- (or odd-) numbered layers are joined by three pairs of H-bonds (N ···O = 2.6 Å and O ···O = 2.6 Å) between metal-coordinated and free hydroxamic acid groups. The intralayer metal-linker interactions and the interlayer H-bonding interactions thus generate a continuously bonded 3D framework. The sum of both types of interactions are essential, as H-bonding interactions on their own would likely not be sufficiently stable as a permanently porous MOF (due to the presumed weakness of H-bonding interactions).

An inspection of the Fe-HAF-2 structure shows that the adjacent even-numbered layers (N and N+2 in Fig. 4b) are also connected to one another by an odd-numbered layer (N+1 in Fig. 4b) that spans the N-to-N+2 interface. This interpenetration by the N+1 layer is stabilized by a combination of non-covalent interactions: first, the terminal phenyl groups of each linker in the N+1 layer form π-π interactions (highlighted in purple in Fig. 4b) with the terminal phenyl groups in the N and N+2 layers. These interactions yield a continuous, staggered π-stacking pattern directed along the *c* axis, creating a double wall that surrounds the hexagonal pores. Second, the two free hydroxamic acid groups in each linker in the N+1 layer form additional H-bonds with the metal-coordinated hydroxamate groups in the N and N+2 layers while the metal-coordinated hydroxamate groups in the same linker are H-bonded to free hydroxamate groups in the N and N+2 layers (N ···O = 3.2 Å) (Fig. 4b). In combination, the π-π and the H-bonding interactions afford a cooperative network of non-covalent bonds of remarkably high density along the *c* axis (Fig. 4c). In fact, each Fe-tris-hydroxamate node (or SBU) is involved in a total of nine H-bonds to the surrounding free hydroxamic acid groups through the participation of six coordinated oxygen atoms and three uncoordinated nitrogen atoms from the three hydroxamate groups (Fig. 4c). To the best of our knowledge, this is the first observation of an SBU-templated H-bonding network within MOFs, which involves all twelve heteroatoms on each TPTH linker. Although there are MOFs featuring free carboxylic acid groups that participate in secondary H-bonds, these interactions are limited in terms of their valency and not crucial for the overall stability of the framework.[52] Ultimately, the increased "bite angle" of hydroxamic acid and its elevated pK_a compared to the carboxylic acid group is responsible for its ability to participate in more extensive H-bonding interactions.

Comparison of the Fe-HAF-2 and Fe-HAF-1 Structures.

With the detailed structure of Fe-HAF-2 in hand, we can attempt to rationalize why it is not isoreticular with its cubic predecessor Fe-HAF-1, which is formed exclusively through bidentate Fe-hydroxamate coordination bonds between BPTH linkers. Given that both Fe-HAF-1 and Fe-HAF-2 are obtained under similar solvothermal synthesis conditions, they likely both represent thermodynamic products that minimize the total free energy of bonds formed in the lattice. It then follows that the total aggregate free energy of π-π and H-bonding interactions in Fe-HAF-2 must be more favorable than the total free energy of Fe^{3+}-hydroxamate interactions that are foregone (two per TPTH linker) by not forming a cubic lattice. On a per-linker basis, the new bonds made in Fe-HAF-2 compared to Fe-HAF-1 amount to one phenyl-phenyl π-π stacking interaction (two total aromatic π-π interactions shared by two linkers) and six H-bonds (twelve total unique H-bonds shared with an

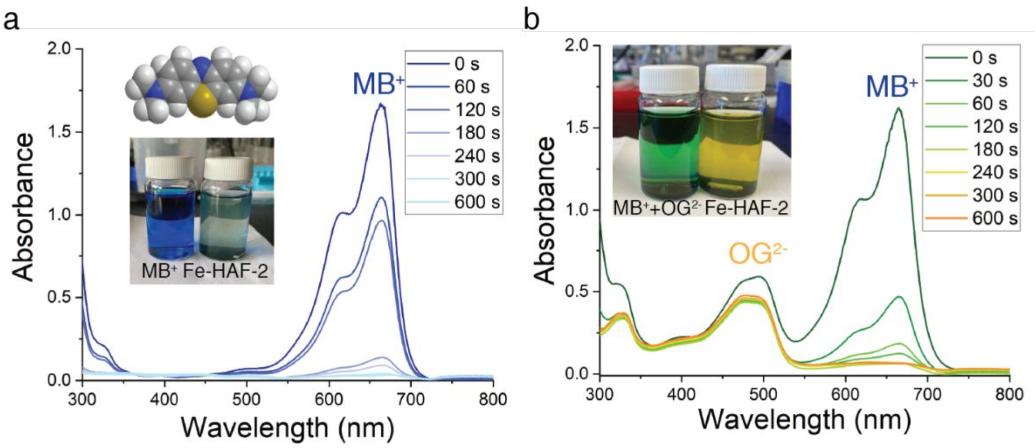

Fig. 6 Dye uptake experiments using a) 10 ppm of MB^+, b) 10 ppm of OG^{2-} and MB^+ in 20 mL H_2O in the presence of 5 mg Fe-HAF-2 over 10 min, monitored by UV-visible spectroscopy.

adjacent linker), which must overcome the loss of two bidentate Fe^{3+}-hydroxamate bonds. Metal-coordination interactions (41–125 kJ/mol)[56] (particularly those of Fe-hydroxamate chelates) are found to be considerably stronger than a similar number of π-π (<10 kJ/mol)[57] and H-bonding interactions (4–8 kJ/mol)[58]. Thus, the inability of TPTH to form an isoreticular cubic lattice as BPTH appears to defy conventional intuition. In the absence of an accurate knowledge on the energetic contributions of individual metal coordination and non-covalent bonds, particularly in the context of an extended 3D lattice, we ascribe the thermodynamic favorability of the trigonal Fe-HAF-2 lattice to the extensive cooperativity/synergy between the π-π and H-bonding interactions (Fig. 4c).

The converse question of why BPTH does not form an isoreticular, trigonal lattice as TPTH is easier to explain. BPTH can theoretically form the same layered, 3D arrangement shown in Fig. 4a (obtained through H-bonding between N and N+2 layers). Yet, the biphenyl linker is not sufficiently long to span across the adjacent even numbered layers to enable interpenetration through π-π and H-bonding interactions, which renders the metal-only interconnected cubic lattice the most thermodynamically favorable option.

Stability of M-HAF-2.

We next examined how the unusual bonding network of M-HAF-2 affected its physical and chemical stability, particularly in aqueous environments. The thermal stability of M-HAF-2 was evaluated by TGA and *in situ* variable temperature PXRD. The TGA curves displayed no significant weight loss up to 200 °C for all three samples (Fig. S6). The PXRD patterns (Fig. 5a and Fig. S7) indicated that M-HAF-2 frameworks retained their crystallinity up to at least 175 °C (the instrument limit), which is consistent with the TGA results. Notably, M-HAF-2 also demonstrated excellent chemical stability in a wide range of aqueous solutions and pH values. As shown in Fig. 5b, Fe-HAF-2 remained crystalline under both highly acidic conditions (pH 1) and basic conditions (pH 13). Compared to Fe-HAF-1, Fe-HAF-2 was found to be slightly less stable under basic conditions compared to Fe-HAF-1 (which is stable even in 5 M NaOH); we attribute this to the deprotonation of the free hydroxamic acid groups and the resulting loss of H-bonding interactions. Conversely, Fe-HAF-2 maintained its crystalline structure even after immersion into 6 M HNO_3, 9 M H_2SO_4, 6 M HCl, and 6 M acetic acid (Fig. 5b), consistent with the retention of the H-bonding network. The chemical stability of Fe-HAF-2 compares very favorably to the other chemically stable Fe-based MOFs such as Fe-HAF-1,MIL-100[59], PCN-250[60], and PCN-600.[61] Ga-HAF-2 and In-HAF-2 were found to be less chemically stable than Fe-HAF-2, likely owing to the reduced stabilities of Ga^{3+}- and In^{3+}-tris-hydroxamates nodes, but both frameworks maintained crystallinity after soaking in aqueous solutions from pH 2 to 11 for at least 1 week (Fig. S8). These experiments illustrate the high thermal and chemical stability of M-HAF-2 in a range of aqueous environments, suggesting that these materials are chemically robust for potential applications such as aqueous chemical separations or gas adsorption.

Dye uptake of Fe-HAF-2.

The aqueous stability of M-HAF-2, coupled with the presence of non-metal-bound hydroxamate groups, suggested that these MOFs could be well-suited for ionic separations. Zeta potential measurements on Fe-HAF-2 yielded an isoelectric point (pI) of 5.3 (Fig. S9). Above pH 5.3, Fe-HAF-2 becomes negatively charged, indicating that it should have favorable interactions with cationic guest molecules. We chose two cationic organic dyes (Methylene Blue (MB^+), Lauth's Violet (LV^+)), one neutral dye (neutral red (NR)), and two anionic organic dyes (Orange G (OG^{2-}) and Acid Orange 6 ($AO6^-$)) to test the uptake selectivity and capacity of Fe-HAF-2. The sizes of all these dyes are smaller than the diameter of hexagonal pore channels to eliminate any steric limitations for uptake (Fig. S10). As shown in Fig. 6 and S11-12, the cationic species (LV^+ and MLB^+) were sequestered rapidly (within 5 min) by Fe-HAF-2, evidenced by the decrease in the absorbance of the solution, while both anionic dyes (OG^{2-} and $AO6^-$) remained in solution. The neutral dye (NR) was also taken up by Fe-HAF-2, but the process was considerably slower (30 min) compared to the cationic species (Fig. S13). The slower rate of NR uptake can be attributed to its diffusion-limited uptake via π–π interactions between NR and the framework, whereas the cationic dye uptake is driven by both electrostatic interactions and π–π stacking. The selectivity of Fe-HAF-2 to bind cationic dyes over anionic and neutral dyes was further investigated by competition experiments. In a solution of equimolar (0.025 mmol) mixed dyes (MB^+ and OG^{2-}), the Fe-HAF-2 selectively removed more than 95% of the cationic dye (MB^+) from the solution within 10 min while the anionic dye (OG^{2-}) remains the same concentration (Fig. 4b). After dye uptake, the Fe-HAF-2 retained its crystallinity as indicated by PXRD measurements (Fig. S14). Interestingly, Fe-HAF-2 sequestered 99% of the cationic dyes (LV^+ and MB^+) from solution within 10 min, far more rapidly than Fe-HAF-1 and most other reported anionic frameworks.[53, 62] To further explore the adsorption kinetics in Fe-HAF-2, the pseudo-second-order kinetic model[63] was used to fit the adsorption of MB^+ over time with different initial concentrations (Fig. S15). The linear form of the equation is:

$$\frac{t}{q_t} = \frac{1}{h} + \frac{1}{q_e}t \qquad (1)$$

with

$$h = k_2\, q_e^2 \qquad (2)$$

where h is the initial sorption rate; t is the adsorption time (s), q_e and q_t are the amount of dye adsorbed at equilibrium and at time t respectively (mg·g⁻¹), and k_2 is the rate constant for pseudo-second-order adsorption (g·mg⁻¹·s⁻¹). $k_2 = \frac{slope^2}{intercept}$ when the $\frac{t}{q_t}$ is plotted against t. The calculated kinetic constants (k_2) and initial sorption rate (h) are summarized in Table S2. The pseudo second-order model showed a good fit with experimental data (R^2 >0.99) across a series of initial dye concentrations from 10–40 ppm (Fig. S15). The values of $q_{e,cal}$ are also consistent with the experimental values of q_e. This finding suggests that the adsorption kinetics indeed followed the pseudo second-order model. The equilibrium adsorption capacity ($q_{e,cal}$) increased with increasing the initial concentration of MB^+, attributed to the relatively strong driving force of the concentration gradient at high initial concentrations. Additionally, the k_2 values decreased from 4.38×10^{-3} to 7.746×10^{-5} g·mg⁻¹·s⁻¹ with the increase of initial dye concentrations from 10 ppm to 40 ppm, which can be ascribed to the lower competition for the adsorption surface sites at lower concentration. Compared with Fe-HAF-1, the presence of hydrogen bonding network in Fe-HAF-2 enables the pH dependent rapid uptake of cationic dyes that offer new potential for pH-dependent chemical separations in porous materials.

Table 1. Extents of transmetalation of In-HAF-2 based on the ICP-MS of digested MOF samples after PSE upon addition of different amounts of $GaCl_3$

Sample	Metal ratio	Normalized metal ratio after digestion for ICP-MS	Empirical formula of MOF based on ICP-MS	Calculated extent of transmetalation in In-HAF-2
In/Ga-1	In : Ga = 1:1	1: 1.2	$In_{0.94}Ga_{1.06}(TPTH)_3$	53.8%
In/Ga-2	In :Ga = 1:2.5	1: 2.3	$In_{0.61}Ga_{1.39}(TPTH)_3$	69.7%
In/Ga-3	In : Ga = 1:5	1: 3.4	$In_{0.46}Ga_{1.54}(TPTH)_3$	77.1%
In/Ga-4	In : Ga = 1:10	1:14.8	$In_{0.13}Ga_{1.87}(TPTH)_3$	93.5%

Postsynthetic Metal Exchange of M-HAF-2.

The presence of uncoordinated hydroxamate groups led us to examine if they could be modified postsynthetically with metal ions (e.g., additional Fe^{3+}, lanthanide cations) at room temperature. However, PXRD and cRED showed that the structure of the M-HAF-2 samples remained the same even after prolonged treatment with excess metal ions. This indicates the uncoordinated hydroxamate groups are inert to metal coordination (Fig. S16 and S17) because they are tightly sequestered within the cooperative H-bonding framework.

Given the high stability of M-HAF-2, we next considered if the coordinated hydroxamate groups/existing metal nodes in these frameworks can undergo PSE. The PSE of metal centers at SBUs in MOFs is a powerful approach for expanding the scope and functionality of these materials[64-67]. Metal-exchange reactions typically are kinetically and thermodynamically controlled by the stability constants of the substituting cations and the strength of the metal-ligand coordination interaction at the inorganic node. To date, most examples of MOFs have focused on labile SBUs containing soft metal ions that are amenable to transmetalation because they are more prone to hydrolysis and metal replacement.[68-71] In contrast, robust MOFs with SBUs featuring strong metal binding affinities are less likely to undergo metal exchange at the node and can induce the undesired formation of an oxide coating.[72] Interestingly, we found that despite the high chemical and thermal stability of M-HAF-2, the metals in the MOFs are still labile enough to undergo transmetalation while preserving the overall structure and crystallinity.

We first tested the transmetalation of In-HAF-2 in the presence of Ga^{3+} via the PSE approach. This was done by immersing In-HAF-2 in a DEF solution containing $GaCl_3$ at 80 °C for 48 h, followed by multiple wash steps using fresh DEF and acetone to remove the excess metal ions. We observed a color change (from white to ivory) of the bulk powder samples as shown in Fig. 7b. In addition to the observed color change, we further characterized the bulk MOF samples by ICP-MS, SEM, and PXRD. PXRD revealed that the frameworks (In-HAF-2) maintained high crystallinity with no changes in the lattice symmetry (Fig. 7a) after metal exchange with Ga^{3+}. SEM images indicated that the MOF powder retained its rod-shaped

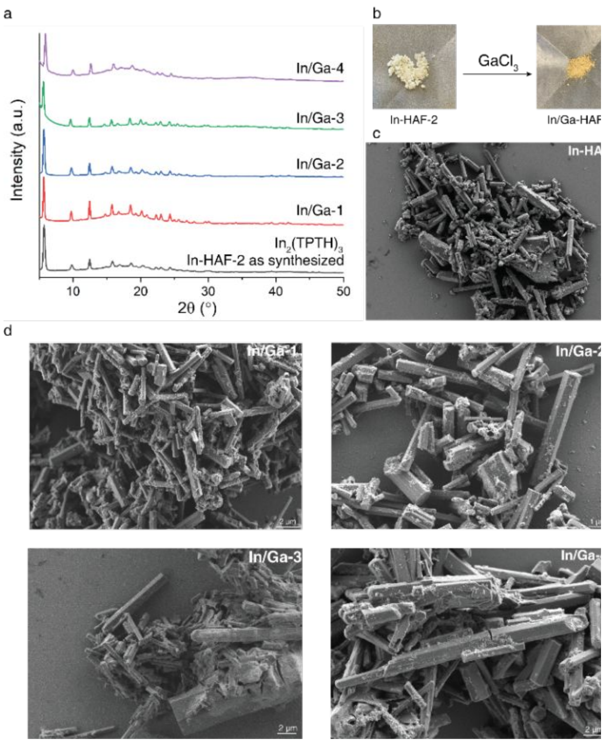

Fig. 7 a) PXRD patterns of In-HAF-2 (as synthesized), In/Ga-1, In/Ga-2, In/Ga-3 and In/Ga-4. b) Photos of In-HAF-2 and In/Ga-4. SEM images of In-HAF-2 (c) and In/Ga-1 to 4 (d).

morphology for all the tested samples (Fig.s 7c, d). As shown in Table 1, the ICP-MS of digested MOF samples after PSE indicate that transmetalation efficiency depends on the metal ratio of In and Ga in reaction, as higher Ga^{3+}:In^{3+} ratios enabled greater degrees of transmetalation. The metal exchange percentage of In/Ga MOF samples varied from 53.8% to 93.5% as the Ga:In metal ratio increased from 1:1 to 10:1 during PSE. It is important to note that the ICP-MS data only reflect the absolute metal concentration in bulk powders, the distribution of metals within individual crystallites requires further study. Moreover, the N_2 sorption of In/Ga-4 after PSE showed a BET surface area of 65 m^2/g (Fig. S18), which is larger than the parent framework (In-HAF-2) and smaller than Ga-HAF-2, further confirming the incomplete transmetalation and potentially reduced stability of In/Ga-4 during the activation process compared with Ga-HAF-2. The In-HAF-2 was also observed to undergo exchange upon treatment with $FeCl_3$ in a concentration-dependent manner without losing the crystalline structure and rod-shaped morphology of the microcrystals (Fig. S19). Significant color change (from white to orange) of the bulk powders was observed (Fig. S19) and the extent of metal exchange was 60%, 76%, 89%, and 89% for MOF samples prepared with In/Fe metal ratios of 1:1, 1:2.5, 1:5 and 1:10, respectively (summarized in Table S3). N_2 adsorption measurements of In/Fe-4 revealed a BET surface area of 97 m^2/g (Fig. S20). Similarly, the transmetalation of Ga-HAF-2 with Fe^{3+} was also possible (summarized in Table S4), but the framework was found to lose crystallinity at high Fe/Ga ratios (Fig. S21). It is worth noting that the incomplete transmetalation has been commonly observed in other mixed-metal-MOF systems using PSE strategy.[73] These results demonstrate that M-HAF-2 can undergo facile metal PSE, which stems from their robust non-covalent bonding frameworks that help maintain the lattice structure during metal substitution reactions. M-HAF-2 also represents one of the few MOFs that can undergo PSE metathesis between trivalent metal ions.[69, 74]

Conclusions

In summary, we have developed a new series of hydroxamate-based MOFs, M-HAF-2 (M = Fe, Ga, In), by using a tetratopic hydroxamate-based linker, H_4TPTH. The M-HAF-2 frameworks are formed through a highly cooperative, protein-like network of metal-linker coordination, π–π, and H-bonding interactions. The interplay between these interactions is manifested by an unusual topology of interpenetrated **hcb**-a net, instead of the originally expected isoreticular expansion of Fe-HAF-1. The M-HAF-2 MOFs exhibits high thermal and chemical stability in a range of aqueous environments and demonstrates Fighighly selective and rapid uptake of dye molecules in a charge-selective fashion. Moreover, the synergistic effect of three different types of interactions within M-HAF-2 gives rise to a highly robust bonding framework that enables facile metal PSE at the single-metal nodes without structural collapse. Overall, our study shows the great utility of new, non-canonical metal-coordinating functionalities such as the hydroxamic acid in the discovery of new bonding and topological patterns in MOFs.

Author Contributions

‡J. Z. and L. S. contributed equally. All authors have given approval to the final version of the manuscript.

J.Z. carried out most of the synthetic work, chemical and structural characterization, and uptake studies and co-wrote the manuscript.

L.S. carried out electron diffraction experiments and structural analysis.

M. K. and R. E. S. carried out BET/gas uptake measurements.

J. A. C. and J. B. B. conducted the original linker synthesis and initial structural characterization.

Z. Z. conducted SEM measurements.

C-J. Yu assisted with illustrations.

S. M. C. oversaw data analysis and co-wrote the paper.

X. Z. and Z. H. oversaw and directed electron diffraction experiments and structural analysis.

F. A. T. directed the project and co-wrote the paper.

Conflicts of interest

There are no conflicts to declare.

Acknowledgements

We thank Dr. Ling Zhang and Dr. Rohit H. Subramanian for zeta potential and SEM experiments. The authors acknowledge the use of ICP-MS facility within the UC Center for Environmental Implications of Nanotechnology in CNSI at UCLA. This work and J.Z., J.B.B., and F.A.T. were primarily supported by the U.S. Department of Energy (DOE) (Division of Materials Sciences, Office of Basic Energy Sciences; DE-SC0003844 for ligand and MOF synthesis and characterization). Additional support was provided by the Swedish Research Council Formas (2020-00831, Z.H.), the Swedish Research Council (VR, 2016-04625, Z.H and 2017-04321, X.Z.) and the Knut and Alice Wallenberg Foundation (KAW, 2016.0072) for ED measurements and analysis and by the DOE (Division of Materials Science and Engineering, DE-FG02-08ER46519 to S.M.C., M.K. and R.E.S for additional MOF characterization).

Notes and references

1. O. M. Yaghi; M. J. Kalmutzki; C. S. Diercks; Introduction to Reticular Chemistry: Metal-Organic Frameworks and Covalent Organic Frameworks, John Wiley & Sons, 2019.

2. H.-C. Zhou; J. R. Long; O. M. Yaghi; *Chem. Rev.*, 2012, **112**, 673-674.

3. P. Z. Moghadam, A. Li, S. B. Wiggin, A. Tao, A. G. P. Maloney, P. A. Wood, S. C. Ward and D. Fairen-Jimenez, *Chem. Mater.*, 2017, **29**, 2618-2625.

4. H. Li, L. Li, R.-B. Lin, W. Zhou, Z. Zhang, S. Xiang and B. Chen, *EnergyChem*, 2019, **1**, 100006.

5. C. Petit, *Curr. Opin. Chem. Eng.*, 2018, **20**, 132-142.

6. H. Li, K. Wang, Y. Sun, C. T. Lollar, J. Li and H.-C. Zhou, *Mater. Today*, 2018, **21**, 108-121.

7. P.-Q. Liao, N.-Y. Huang, W.-X. Zhang, J.-P. Zhang and X.-M. Chen, *Science*, 2017, **356**, 1193-1196.

8. J. Della Rocca, D. Liu and W. Lin, *Acc. Chem. Res.*, 2011, **44**, 957-968.

9. M.-X. Wu and Y.-W. Yang, *Adv. Mater.*, 2017, **29**, 1606134.

10. E. A. Dolgopolova, A. M. Rice, C. R. Martin and N. B. Shustova, *Chem. Soc. Rev.*, 2018, **47**, 4710-4728.

11. M. R. Tchalala, P. M. Bhatt, K. N. Chappanda, S. R. Tavares, K. Adil, Y. Belmabkhout, A. Shkurenko, A. Cadiau, N. Heymans, G. De Weireld, G. Maurin, K. N. Salama and M. Eddaoudi, *Nat. Commun.*, 2019, **10**, 1328.

12. P.-Q. Liao, J.-Q. Shen and J.-P. Zhang, *Coord. Chem. Rev.*, 2018, **373**, 22-48.

13. T. A. Goetjen, J. Liu, Y. Wu, J. Sui, X. Zhang, J. T. Hupp and O. K. Farha, *Chem. Commun.*, 2020, **56**, 10409-10418.

14. J. Zhu, P. M. Usov, W. Xu, P. J. Celis-Salazar, S. Lin, M. C. Kessinger, C. Landaverde-Alvarado, M. Cai, A. M. May, C. Slebodnick, D. Zhu, S. D. Senanayake and A. J. Morris, *J. Am. Chem. Soc.*, 2018, **140**, 993-1003.

15. L. Feng, K.-Y. Wang, G. S. Day, M. R. Ryder and H.-C. Zhou, *Chem. Rev.*, 2020, **120**, 13087-13133.

16. N. L. Rosi, J. Eckert, M. Eddaoudi, D. T. Vodak, J. Kim, M. O'Keeffe and O. M. Yaghi, *Science*, 2003, **300**, 1127-1129.

17. C. Serre, F. Millange, C. Thouvenot, M. Noguès, G. Marsolier, D. Louër and G. Férey, *J. Am. Chem. Soc.*, 2002, **124**, 13519-13526.

18. G. Férey, C. Mellot-Draznieks, C. Serre, F. Millange, J. Dutour, S. Surblé and I. Margiolaki, *Science*, 2005, **309**, 2040-2042.

19. J. H. Cavka, S. Jakobsen, U. Olsbye, N. Guillou, C. Lamberti, S. Bordiga and K. P. Lillerud, *J. Am. Chem. Soc.*, 2008, **130**, 13850-13851.

20. J. E. Mondloch, W. Bury, D. Fairen-Jimenez, S. Kwon, E. J. DeMarco, M. H. Weston, A. A. Sarjeant, S. T. Nguyen, P. C. Stair, R. Q. Snurr, O. K. Farha and J. T. Hupp, *J. Am. Chem. Soc.*, 2013, **135**, 10294-10297.

21. D. Yuan, D. Zhao, D. Sun and H.-C. Zhou, *Angew. Chem. Int. Ed.*, 2010, **49**, 5357-5361.

22. V. Guillerm and M. Eddaoudi, *Acc. Chem. Res.*, 2021, **54**, 3298-3312.

23. P. F. Muldoon, C. Liu, C. C. Miller, S. B. Koby, A. Gamble Jarvi, T.-Y. Luo, S. Saxena, M. O'Keeffe and N. L. Rosi, *J. Am. Chem. Soc.*, 2018, **140**, 6194-6198.

24. R.-J. Li, M. Li, X.-P. Zhou, D. Li and M. O'Keeffe, *Chem. Commun.*, 2014, **50**, 4047-4049.

25. D.-X. Xue, A. Cadiau, Ł. J. Weseliński, H. Jiang, P. M. Bhatt, A. Shkurenko, L. Wojtas, C. Zhijie, Y. Belmabkhout, K. Adil and M. Eddaoudi, *Chem. Commun.*, 2018, **54**, 6404-6407.

26. V. Guillerm, Ł. J. Weseliński, Y. Belmabkhout, A. J. Cairns, V. D'Elia, Ł. Wojtas, K. Adil and M. Eddaoudi, *Nat. Chem.*, 2014, **6**, 673-680.

27. A. E. Martell, *Pure Appl. Chem.*, 1968, **17**, 129-178.

28. P. J. Almhjell and J. H. Mills, *Curr. Opin. Struct. Biol.*, 2018, **51**, 170-176.

29. B. F. Abrahams, T. A. Hudson, L. J. McCormick and R. Robson, *Cryst. Growth Des.*, 2011, **11**, 2717-2720.

30. K. Nakabayashi and S.-i. Ohkoshi, *Inorg. Chem.*, 2009, **48**, 8647-8649.

31. M. Shota, Y. Teppei and K. Hiroshi, *Chem. Lett.*, 2009, **38**, 654-655.

32. B. F. Abrahams, J. Coleiro, K. Ha, B. F. Hoskins, S. D. Orchard and R. Robson, *J. Chem. Soc., Dalton Trans.*, 2002, **(8)**, 1586-1594.

33. M. Hmadeh, Z. Lu, Z. Liu, F. Gándara, H. Furukawa, S. Wan, V. Augustyn, R. Chang, L. Liao, F. Zhou, E. Perre, V. Ozolins, K. Suenaga, X. Duan, B. Dunn, Y. Yamamto, O. Terasaki and O. M. Yaghi, *Chem. Mater.*, 2012, **24**, 3511-3513.

34. N. T. T. Nguyen, H. Furukawa, F. Gándara, C. A. Trickett, H. M. Jeong, K. E. Cordova and O. M. Yaghi, *J. Am. Chem. Soc.*, 2015, **137**, 15394-15397.

35. R. Matheu, E. Gutierrez-Puebla, M. Á. Monge, C. S. Diercks, J. Kang, M. S. Prévot, X. Pei, N. Hanikel, B. Zhang, P. Yang and O. M. Yaghi, *J. Am. Chem. Soc.*, 2019, **141**, 17081-17085.

36. J. Liu, Y. Zhou, Z. Xie, Y. Li, Y. Liu, J. Sun, Y. Ma, O. Terasaki and L. Chen, *Angew. Chem. Int. Ed.*, 2020, **59**, 1081-1086.

37. A. L. Crumbliss, *Coord. Chem. Rev.*, 1990, **105**, 155-179.

38. R. Saha, N. Saha, R. S. Donofrio and L. L. Bestervelt, *J. Basic Microbiol.*, 2013, **53**, 303-317.

39. D. Al Shaer, O. Al Musaimi, B. G. de la Torre and F. Albericio, *Eur. J. Med. Chem.*, 2020, **208**, 112791.

40. J. B. Neilands, *Science*, 1967, **156**, 1443-1447.

41. K. Sugamata, C. Takagi, K. Awano, T. Iihama and M. Minoura, *Dalton Trans.*, 2020, **49**, 9948-9952.

42. J. A. Chiong, J. Zhu, J. B. Bailey, M. Kalaj, R. H. Subramanian, W. Xu, S. M. Cohen and F. A. Tezcan, *J. Am. Chem. Soc.*, 2020, **142**, 6907-6912.

43. N. M. Padial, J. Castells-Gil, N. Almora-Barrios, M. Romero-Angel, I. da Silva, M. Barawi, A. García-Sánchez, V. A. de la Peña O'Shea and C. Martí-Gastaldo, *J. Am. Chem. Soc.*, 2019, **141**, 13124-13133.

44. C. F. Pereira, A. J. Howarth, N. A. Vermeulen, F. A. Almeida Paz, J. P. C. Tomé, J. T. Hupp and O. K. Farha, *Mater. Chem. Front.*, 2017, **1**, 1194-1199.

45. T. Beissel, R. E. Powers and K. N. Raymond, *Angew. Chem. Int. Ed.*, 1996, **35**, 1084-1086.

46. Y.-N. Gong, D.-C. Zhong and T.-B. Lu, *CrystEngComm*, 2016, **18**, 2596-2606.

47. R.-B. Lin, Y. He, P. Li, H. Wang, W. Zhou and B. Chen, *Chem. Soc. Rev.*, 2019, **48**, 1362-1389.

48. P. Li, M. R. Ryder and J. F. Stoddart, *Acc. Mater. Res.*, 2020, **1**, 77-87.

49. B. Wang, R.-B. Lin, Z. Zhang, S. Xiang and B. Chen, *J. Am. Chem. Soc.*, 2020, **142**, 14399-14416.

50. J. Luo, J.-W. Wang, J.-H. Zhang, S. Lai and D.-C. Zhong, *CrystEngComm*, 2018, **20**, 5884-5898.

51. I. Hisaki, C. Xin, K. Takahashi and T. Nakamura, *Angew. Chem. Int. Ed.*, 2019, **58**, 11160-11170.

52. C. Marsh, X. Han, J. Li, Z. Lu, S. P. Argent, I. da Silva, Y. Cheng, L. L. Daemen, A. J. Ramirez-Cuesta, S. P. Thompson, A. J. Blake, S. Yang and M. Schröder, *J. Am. Chem. Soc.*, 2021, **143**, 6586-6592.

53. M. N. Ahamad, M. S. Khan, M. Shahid and M. Ahmad, *Dalton Trans.*, 2020, **49**, 14690-14705.

54. M. O. Cichocka, J. Ångström, B. Wang, X. Zou and S. Smeets, *J Appl Crystallogr*, 2018, **51**, 1652-1661.

55. Z. Huang, E. S. Grape, J. Li, A. K. Inge and X. Zou, *Coord. Chem. Rev.*, 2021, **427**, 213583.

56. S. Leininger, B. Olenyuk and P. J. Stang, *Chem. Rev.*, 2000, **100**, 853-908.

57. Y. Zhao and D. G. Truhlar, *J. Chem. Theory Comput.*, 2007, **3**, 289-300.

58. K. Wendler, J. Thar, S. Zahn and B. Kirchner, *J. Phys. Chem. A*, 2010, **114**, 9529-9536.

59. C. R. Quijia, C. Lima, C. Silva, R. C. Alves, R. Frem and M. Chorilli, *J. Drug Delivery Sci. Technol.*, 2021, **61**, 102217.

60. D. Feng, K. Wang, Z. Wei, Y.-P. Chen, C. M. Simon, R. K. Arvapally, R. L. Martin, M. Bosch, T.-F. Liu, S. Fordham, D. Yuan, M. A. Omary, M. Haranczyk, B. Smit and H.-C. Zhou, *Nat. Commun.*, 2014, **5**, 5723.

61. K. Wang, D. Feng, T.-F. Liu, J. Su, S. Yuan, Y.-P. Chen, M. Bosch, X. Zou and H.-C. Zhou, *J. Am. Chem. Soc.*, 2014, **136**, 13983-13986.0

62. V. K.-M. Au, *Front. Chem.*, 2020, **8** (708).

63. L. Ai, C. Zhang and L. Meng, *J. Chem. Eng. Data*, 2011, **56**, 4217-4225.

64. X. Song, T. K. Kim, H. Kim, D. Kim, S. Jeong, H. R. Moon and M. S. Lah, *Chem. Mater.*, 2012, **24**, 3065-3073.

65. M. Kalaj and S. M. Cohen, *ACS Cent. Sci.*, 2020, **6**, 1046-1057.

66. S. Seth, G. Savitha and J. N. Moorthy, *J. Mater. Chem. A*, 2015, **3**, 22915-22922.

67. S. Abednatanzi, P. Gohari Derakhshandeh, H. Depauw, F.-X. Coudert, H. Vrielinck, P. Van Der Voort and K. Leus, *Chem. Soc. Rev.*, 2019, **48**, 2535-2565.

68. S. Das, H. Kim and K. Kim, *J. Am. Chem. Soc.*, 2009, **131**, 3814-3815.

69. C. K. Brozek and M. Dincă, *J. Am. Chem. Soc.*, 2013, **135**, 12886-12891.

70. N. M. Padial, B. Lerma-Berlanga, N. Almora-Barrios, J. Castells-Gil, I. da Silva, M. a. de la Mata, S. I. Molina, J. Hernández-Saz, A. E. Platero-Prats, S. Tatay and C. Martí-Gastaldo, *J. Am. Chem. Soc.*, 2020, **142**, 6638-6648.

71. J. Yang, X. Wang, F. Dai, L. Zhang, R. Wang and D. Sun, *Inorg. Chem.*, 2014, **53**, 10649-10653.

72. M. S. Denny, L. R. Parent, J. P. Patterson, S. K. Meena, H. Pham, P. Abellan, Q. M. Ramasse, F. Paesani, N. C. Gianneschi and S. M. Cohen, *J. Am. Chem. Soc.*, 2018, **140**, 1348-1357.

73. M. Y. Masoomi, A. Morsali, A. Dhakshinamoorthy and H. Garcia, *Angew. Chem. Int. Ed.*, 2019, **58**, 15188-15205.

74. T.-F. Liu, L. Zou, D. Feng, Y.-P. Chen, S. Fordham, X. Wang, Y. Liu and H.-C. Zhou, *J. Am. Chem. Soc.*, 2014, **136**, 7813-7816.
.